



Generation and distribution of atomic entanglement in coupled-cavity arrays

J. P. Mendonça ^{*}, F. A. B. F. de Moura, M. L. Lyra, and G. M. A. Almeida
Instituto de Física, Universidade Federal de Alagoas, 57072-900 Maceió, AL, Brazil

 (Received 30 May 2020; revised 30 November 2020; accepted 7 December 2020; published 21 December 2020)

We study the dynamics of entanglement in a one-dimensional coupled-cavity array, with each cavity containing a two-level atom, via the Jaynes-Cummings-Hubbard (JCH) Hamiltonian in the single-excitation sector. The model features a rich variety of dynamical regimes that can be harnessed for entanglement control. The protocol is based on setting an excited atom above the ground state and further letting it evolve following the natural dynamics of the Hamiltonian. Here we focus on the concurrence between pairs of atoms and its relation to atom-field correlations and the involved free-field modes. We show that the extension and distribution pattern of pairwise entanglement can be manipulated through a judicious tuning of the atom-cavity coupling strength. By also including static noise in the cavity frequencies, we explore the onset of Anderson localization and its interplay with the atomic trapping known to take place in the strong-hopping regime. Remarkably, we find that the stronger the disorder is, the higher are the atom-field correlations, whereas the atomic concurrence responds nonmonotonically. Overall, our work offers a comprehensive account of the machinery of the single-excitation JCH Hamiltonian and contributes to the design of hybrid light-matter quantum networks.

DOI: [10.1103/PhysRevA.102.062416](https://doi.org/10.1103/PhysRevA.102.062416)

I. INTRODUCTION

Quantum entanglement is one of the most intriguing properties of nature with no classical analog [1]. It is a key manifestation in many-body physics for it plays a significant role in quantum phase transitions [2–4]. In addition, entanglement is a fundamental resource in quantum information processing tasks such as teleportation [5], quantum cryptography [6,7], and quantum dense coding [8], to name a few. In this respect, in order to properly design such a class of protocols, one must be able to faithfully transmit quantum states and establish entanglement over arbitrarily distant parties (qubits) [9,10]. Setting reliable quantum communication channels is thus a primary step towards building large-scale quantum networks [11,12].

Along those lines, photonic channels stand out as current technology allows for light propagation over large distances with negligible decoherence. In addition, local quantum information processing units (nodes) may consist of single atoms placed in optical resonators. This allows for light-matter interfacing with a high degree of control, thanks to experimental advances in cavity-QED-based architectures [13–16].

A paradigmatic framework to deal with coupled-cavity systems is the Jaynes-Cummings-Hubbard (JCH) model, where cavities containing single two-level atoms are brought together enough to allow for photon tunneling. Atom-cavity coupling is given by the acclaimed Jaynes-Cummings interaction in the rotating-wave approximation. Early developments of the model began with the discovery that it displays a superfluid to Mott insulator quantum phase transition [17–19]. This established coupled-cavity systems also as potential many-body quantum simulators [20]. Furthermore, the hybrid

light-matter nature of the excitations unveils novel phases of matter [21] and can be useful for quantum information processing tasks [22,23] (for reviews of the model and related content, see Refs. [20,24]).

In this work, we further explore the versatility of a one-dimensional (1D) coupled-cavity array in order to generate and distribute entanglement, which is a key element in the design of quantum networks [11]. The protocol is based on preparing an impurity—here, an excited atom—over a well-defined ground state and letting it evolve following the natural, Hamiltonian dynamics of the system. Along the process, it is possible to generate entanglement, as shown for spin chains in Refs. [25,26] (cf. [27] for an experimental realization). Here the initial atomic excitation is released from the middle of a coupled-cavity array prepared in the vacuum state (no photons) with all the remaining atoms in their ground state. As the JCH model commutes with the total number operator, the dynamics ends up being restricted to the single-excitation subspace which allows for easy analytical treatment [28] in addition to displaying very rich properties [23,26,28,29].

We carry out a detailed analysis over limiting interaction regimes of the JCH Hamiltonian and track entanglement evolution over time in two forms: the von Neumann entropy for the whole atomic component in regard to the photonic degrees of freedom and the concurrence between atomic pairs. We discuss the role of atom-field entropy in establishing atomic entanglement and how its spatial distribution profile is related to the atom-cavity interaction strength and the field normal modes. The response of those quantities to disorder taking place in the cavity frequencies across the array is also addressed and we find that it can actually assist entanglement generation as Anderson localization [30] allows for maximum atom-field entropy in the strong-hopping regime, in contrast to the ordered array, where an atomic trapping [23,28,29] occurs due to the spatial profile of modes involved in the dynamics.

^{*}jpedromend@gmail.com

In Sec. II, we introduce the JCH Hamiltonian. In Sec. III, the weak- and strong-hopping regimes of the model are addressed in detail. In Sec. IV, we outline the entanglement signatures of interest and discuss their dynamics, focusing on those limiting regimes. Conclusions are drawn in Sec. V.

II. JAYNES-CUMMINGS-HUBBARD MODEL

We consider a one-dimensional array of N high-quality coupled cavities, each containing a single two-level atom, with $|g\rangle$ and $|e\rangle$ denoting the ground and excited states, respectively. Each atom interacts with the field through the local Jaynes-Cummings (JC) Hamiltonian (in the rotating-wave approximation) [31],

$$H_x^{\text{JC}} = \omega_c a_x^\dagger a_x + \omega_a \sigma_x^+ \sigma_x^- + g(\sigma_x^+ a_x + \sigma_x^- a_x^\dagger), \quad (1)$$

where a_x^\dagger (a_x) and σ_x^+ (σ_x^-) are, respectively, the bosonic and atomic raising (lowering) operators acting on the x th cavity, g is the atom-field coupling strength, ω_c is the cavity frequency, and ω_a is the atomic transition frequency. We set $\hbar = 1$ for convenience. The eigenstates of Hamiltonian (1) are dressed (hybrid) states featuring photonic and atomic excitations known as polaritons, which in resonance ($\Delta = \omega_c - \omega_a = 0$) read $|n\pm\rangle_x = (|g, n\rangle_x \pm |e, n-1\rangle_x)/\sqrt{2}$ with energies $E_n^\pm = n\omega_c \pm g\sqrt{n}$, where $|n\rangle_x$ denotes a n -photon Fock state at the x th cavity. Note that the vacuum state $|g, 0\rangle_x$ is also an eigenstate, with zero energy.

We now assume that the local cavity modes overlap in such a way to allow photonic tunneling in a uniform array. This coupled-cavity system is described by the JCH Hamiltonian

$$H = \sum_{x=1}^N H_x^{\text{JC}} - J \sum_{x=1}^{N-1} (a_{x+1}^\dagger a_x + \text{H.c.}), \quad (2)$$

with J being the photon tunneling. The above Hamiltonian acts on basis states of the form $\bigotimes_{x=1}^N |s, n\rangle_x$, with $s \in \{g, e\}$. Sorting out these states according to the total excitation number, the Hamiltonian (2) can be expressed by $H = \text{diag}[H^{(0)}, H^{(1)}, H^{(2)}, \dots]$, where $H^{(j)}$ denotes the Hamiltonian matrix spanned on basis states featuring a fixed number j of excitations.

Here we focus on the generation of entanglement out of localized atomic state $|e\rangle_i$ with all the remaining atoms in their ground state and no photons. In both cases, the system dynamics is restricted to the single-excitation subspace, $H^{(1)}$, which is spanned by $|1_x\rangle \equiv \hat{a}_x^\dagger |\emptyset\rangle$ and $|e_x\rangle \equiv \hat{\sigma}_x^+ |\emptyset\rangle$, with $|\emptyset\rangle \equiv |\text{vac}\rangle|g\rangle_1 \cdots |g\rangle_N$, where the former denotes a single photon at the x th cavity and the latter represents the x th atom excited. The Hilbert-space dimension is thus twice the number of cavities.

In general, the Hamiltonian (2) yields rich dynamics even in the single-excitation sector [22,23,28]. In the following, we address two limiting regimes of interest that will help us to visualize the entanglement dynamics afterwards.

III. INTERACTION REGIMES IN THE SINGLE-EXCITATION SECTOR

First, we recall that when the atom-field interaction strength g and the atomic transition frequency ω_a are uniform

across the array, the Hamiltonian (2) can be rearranged as a sum of N decoupled JC-like interactions, $H = \sum_k H_k$, in terms of normal modes, where [23,28,29,32]

$$H_k = \omega_k \alpha_k^\dagger \alpha_k + \omega_a \beta_k^\dagger \beta_k + g(\alpha_k^\dagger \beta_k + \beta_k^\dagger \alpha_k), \quad (3)$$

and $\alpha_k^\dagger \equiv |\alpha_k\rangle\langle\emptyset|$ ($\beta_k^\dagger \equiv |\beta_k\rangle\langle\emptyset|$) is the field (atomic) normal-mode operator. In other words, $\{|\alpha_k\rangle\}$ is the set of N eigenstates of the hopping (free-field) Hamiltonian, with eigenvalues $\{\omega_k\}$, each having the form $|\alpha_k\rangle = \sum_x v_{k,x} |1_x\rangle$. The atomic states $|\beta_k\rangle$ are set with the very same spatial profile (amplitudes) as their photonic counterpart, that is, $|\beta_k\rangle = \sum_x v_{k,x} |e_x\rangle$, but all lying at the same frequency ω_a . Although we are dealing with a uniform pattern of hopping rates, the above situation is valid regardless of the embedded adjacency matrix. Therefore, the model can be solved analytically once one knows the whole free-field spectral decomposition. Indeed, since the above Hamiltonian is a 2×2 block-diagonal matrix indexed by k , its eigenstates are found to be [23,29]

$$|\psi_k^\pm\rangle = A_k^\pm |\alpha_k\rangle + B_k^\pm |\beta_k\rangle, \quad (4)$$

where

$$A_k^\pm = \frac{2g}{\sqrt{(\Delta_k \pm \Omega_k)^2 + 4g^2}}, \quad B_k^\pm = \frac{\Delta_k \pm \Omega_k}{\sqrt{(\Delta_k \pm \Omega_k)^2 + 4g^2}}, \quad (5)$$

$\Delta_k = \omega_a - \omega_k$ is the detuning between the atomic and the field normal-mode frequency, and $\Omega_k = \sqrt{\Delta_k^2 + 4g^2}$ is the corresponding vacuum Rabi frequency. The energy levels are given by

$$\varepsilon_k^{(\pm)} = \frac{1}{2} (\omega_a + \omega_k \pm \Omega_k). \quad (6)$$

The JCH Hamiltonian written in the form of effective JC interactions [see Eq. (3)] allows for a convenient visualization of the system's behavior, as shown in Fig. 1(c). One of the most interesting features is the possibility of setting up a particular mode to trigger a pair of dressed JC-like states [cf. Eq. (4)]. This can be done in the strong-hopping regime, $g \ll J$, upon a judicious tuning of the atomic frequency ω_a . In order to see this, let us move on to the interaction picture,

$$H^I(t) = g \left(\sum_k \alpha_k^\dagger \beta_k e^{-i\Delta_k t} + \text{H.c.} \right). \quad (7)$$

Setting ω_a in resonance with a given mode, say k' , one of the terms becomes time independent ($\Delta_{k'} = 0$) and, considering $g \ll \{\Delta_{k \neq k'}\}$, all the remaining terms become fast rotating and thus can be ignored. Going back to the Schrödinger picture, we are left with the effective Hamiltonian,

$$H_{\text{eff}} = H_{k'} + \sum_{k \neq k'} (\omega_k \alpha_k^\dagger \alpha_k + \omega_a \beta_k^\dagger \beta_k), \quad (8)$$

where the first term is given by Eq. (3). The above equation describes a single JC-like interaction taking place at mode k' , spanning a pair of fully dressed states $|\psi_{k'}^\pm\rangle$ [cf. Eq. (4)], with all the other atomic and field modes uncoupled. A schematic representation of this regime is shown in Fig. 1(c).

Within the strong-hopping regime, if an atomic excitation is prepared somewhere along the array, say $|\psi(0)\rangle = |e_{x_0}\rangle$, it may get trapped depending on the nature of the free-field

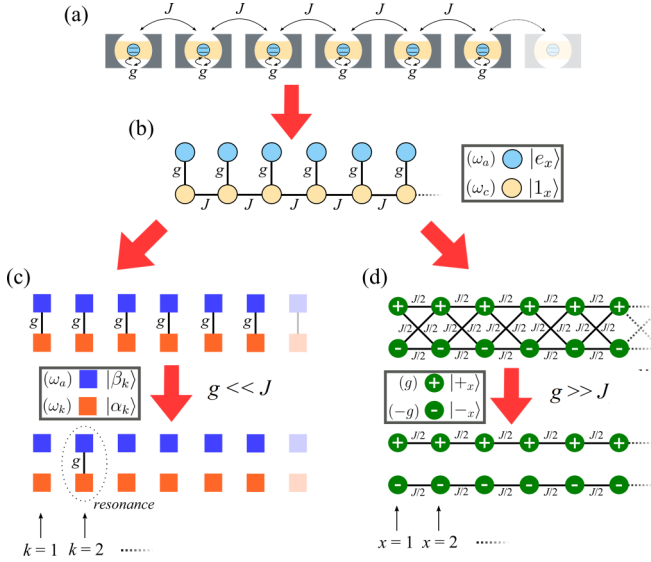


FIG. 1. State-graph structure of the JCH Hamiltonian describing a coupled-cavity system. (a) Sketch of an array featuring a uniform pattern of hopping rates J . Each cavity has frequency ω_c and is coupled to a two-level atom (or qubit) with frequency ω_a through a local atom-field interaction given by g . (b) In the single-excitation sector, the model is reduced to a tight-binding chain (with extra, vertically attached sites) where single-photon states ($\{|1_x\rangle\}$) spread over the array and are eventually converted into atomic degrees of freedom ($\{|e_x\rangle\}$). (c) The JCH Hamiltonian may be expressed in terms of decoupled JC-like interactions between free-field normal modes $\{|\alpha_k\rangle\}$ and its atomic analog $\{|\beta_k\rangle\}$. In the strong-hopping regime ($g \ll J$), proper tuning leads to a single resonant effective interaction (for $k = 2$ in the example). (d) Another form of expressing the JCH Hamiltonian is in terms of local polaritonic states [see Eq. (12)]. Note that here we set $\omega_a = \omega_c = 0$ for visualization purposes. The resulting double interconnected array can be decoupled in the weak-hopping regime ($g \gg J$) by dropping out fast rotating terms. In this particular case, we have a standard tight-binding structure for each polaritonic branch having exactly the same dispersion law of the embedded coupled-cavity array with the hopping rate rescaled to $J/2$.

spectrum and resonance conditions [22,23,28,29]. In the off-resonant case, that is $\omega_a \neq \omega_k$ for all k , it is immediate to note that $|\psi(t)\rangle = e^{-iHt}|\psi(0)\rangle = e^{-i\omega_a t}|e_{x_0}\rangle$ and so the atomic excitation indeed freezes at the initial cavity x_0 . Now, if ω_a is put in narrow resonance with a given (nondegenerate) mode k' , thereby setting up a JC-like interaction between this mode and its atomic counterpart, the evolved atomic coefficients read

$$c_{a,x}(t) = e^{-i\omega_a t} \left[\sum_{k \neq k'} v_{k,x} v_{k',x_0}^* + \cos(gt) v_{k',x} v_{k',x_0}^* \right], \quad (9)$$

and as $\sum_k v_{k,x} v_{k,x_0}^* = 1$ ($= 0$) for $x = x_0$ ($x \neq x_0$) due to orthonormality, the return probability

$$p_{a,x_0}(t) \equiv |c_{a,x_0}(t)|^2 = [1 + |v_{k',x_0}|^2 (\cos gt - 1)]^2. \quad (10)$$

In other words, the amount of information released by the initial excitation ultimately depends on the overlap between $|\beta_{k'}\rangle$ and $|e_{x_0}\rangle$. For a uniform array, which is our case, the free-field spectrum consists of plane waves of the form $v_{k,x} \propto \sin(kx)$, with $k = \pi m / (N + 1)$ and $m = 1, \dots, N$, and so the

overlap should be small enough to retain most of the amplitude. Still, for finite N , some amount of atomic probability periodically flows out of the initial state, reaching the other atomic states in phase as

$$p_{a,x}(t) = |v_{k',x} v_{k',x_0}^*|^2 (\cos gt - 1)^2, \quad (11)$$

for $x \neq x_0$.

Taking the other limit, that is when we increase g/J until reaching the weak-hopping regime [22,28], every normal mode becomes fully dressed and the corresponding eigenstates effectively take the form $|\psi_k^\pm\rangle = (|\alpha_k\rangle \pm |\beta_k\rangle) / \sqrt{2}$. These are extended polaritons that form two single-particle dispersion branches having the very same structure as of an embedded array with the hopping scale redefined by $J/2$ [see Eq. (6)]. A much better way to visualize this is by rewriting the JCH Hamiltonian, given by Eq. (2), in terms of local polaritonic operators $P_x^{(n,\pm)} \equiv |\emptyset\rangle_x \langle n\pm|$ [19]. Dropping out terms with $n \neq 1$, the Hamiltonian becomes

$$\begin{aligned} H = & \sum_{x=1}^N (g^+ P_x^{(+)\dagger} P_x^{(+)} + g^- P_x^{(-)\dagger} P_x^{(-)}) \\ & + \sum_{x=1}^N \frac{\Delta}{2} (P_x^{(+)\dagger} P_x^{(-)} + P_x^{(-)\dagger} P_x^{(+)}) \\ & - \frac{J}{2} \sum_{x=1}^{N-1} (P_x^{(+)\dagger} P_{x+1}^{(+)} + P_x^{(-)\dagger} P_{x+1}^{(-)}) \\ & + P_x^{(+)\dagger} P_{x+1}^{(-)} + P_x^{(-)\dagger} P_{x+1}^{(+)} + \text{H.c.}, \quad (12) \end{aligned}$$

where $P_x^{(\pm)} = P_x^{(1,\pm)}$ for brevity and $g^\pm = (\omega_c + \omega_a)/2 \pm g$. The above Hamiltonian is equivalent to a double tight-binding array connected to each other through the hopping terms that exchange between even ($|+\rangle_x$) and odd ($|-\rangle_x$) polaritons [see Fig. 1(d)]. This can be further simplified when $g \gg J$, Δ , where both chains become effectively decoupled [19,28], i.e., those interconverting terms are fast rotating and can be dropped out. (Note that $\Delta = 0$ yields that $|\pm\rangle_x$ are the states that diagonalize each JC cell, thereby breaking their connection locally despite g .) It is worth mentioning that the even and odd polaritonic operators each obey the same algebra as the spin-1/2 ladder operators. Therefore, in this regime, the JCH Hamiltonian effectively describes an XY spin chain with spin up (down) corresponding to the presence (absence) of polaritons [19,33]. It is worth pointing out that for the large detuning limit $\Delta \gg g, J$ can also be mapped onto a spin chain, except in this case the photonic mode propagates much faster than the atomic one, with the profile of each mode being maintained. More details about this regime can be found in Ref. [28].

In such weak-hopping scenario, the dynamics of the atomic excitation mimics that of a single particle propagating along either of the uncoupled effective chains (it spreads out ballistically in a uniform chain) with hopping constant $J/2$, the only difference being that it is continuously converted back and forth to a photonic state at rate g [28]. Time-evolved atomic coefficients in this case read

$$c_{a,x}(t) = \cos gt \sum_k e^{-i\frac{\omega_k}{2} t} v_{k,x} v_{k,x_0}^*. \quad (13)$$

Also note in Fig. 1(d) that if the system is initialized in an even (odd) polariton state, the odd (even) counterpart will not take part in the dynamics.

IV. ENTANGLEMENT PROPERTIES

Now that we have made an overall analysis of the two main limiting regimes of the JCH model, we are to track the entanglement over time between atomic and photonic degrees of freedom via the von Neumann entropy, as well as between pairs of atoms via the concurrence. Those measures are introduced next.

A. Entanglement measures

The single-excitation subspace is spanned by $\{|1_i\rangle, |e_i\rangle\}$ so that a general state can be written as

$$|\psi\rangle = \sum_{i=1}^N (c_{f,i}|1_i\rangle + c_{a,i}|e_i\rangle), \quad (14)$$

where $c_{f,x}$ and $c_{a,x}$ are the field and atomic coefficients, respectively. In the density-operator formalism, we have

$$\begin{aligned} \rho = |\psi\rangle\langle\psi| = & \sum_{i=1}^N \sum_{j=1}^N (c_{f,i}c_{f,j}^*|1_i\rangle\langle 1_j| + c_{f,i}c_{a,j}^*|1_i\rangle\langle e_j| \\ & + c_{a,i}c_{f,j}^*|e_i\rangle\langle 1_j| + c_{a,i}c_{a,j}^*|e_i\rangle\langle e_j|). \end{aligned} \quad (15)$$

Now, tracing out the cavity (field) modes, $\rho_a = \text{Tr}_f[\rho]$, we obtain

$$\rho_a = \sum_{i=1}^N |c_{f,i}|^2 |\Downarrow\rangle\langle\Downarrow| + \sum_{i=1}^N \sum_{j=1}^N c_{a,i}c_{a,j}^* \sigma_i^+ |\Downarrow\rangle\langle\Downarrow| \sigma_j^-, \quad (16)$$

where $|\Downarrow\rangle \equiv |g\rangle_1 \dots |g\rangle_N$.

Note that in general, ρ_a is a mixed state and thus the atomic component, as a whole, is said to be entangled with the photonic subsystem. The diagonal form of ρ_a has only two entries, $\Pi_f \equiv \sum_i |c_{f,i}|^2$ and $\Pi_a \equiv \sum_i |c_{a,i}|^2$, namely the total photonic and atomic probabilities, respectively. Since $|\psi\rangle$ is a pure state, we can evaluate the amount of entanglement between two partitions through the von Neumann entropy. For the, say, atomic component,

$$\begin{aligned} S[\rho_a] &= -\text{Tr} \rho_a \log_2 \rho_a \\ &= -\Pi_a \log_2 \Pi_a - (1 - \Pi_a) \log_2 (1 - \Pi_a), \end{aligned} \quad (17)$$

which gives 0 (1) for a fully separable (entangled) state. Note that the entropy reaches its maximum for $\Pi_f = \Pi_a = 1/2$, that is, $S_{\text{max}} = -\log_2(1/2) = 1$.

To evaluate bipartite entanglement between the atoms, we choose a pair of sites, say, i and j , and further trace out the rest of them from ρ_a [Eq. (16)] to obtain a four-dimensional reduced matrix spanned in the basis $\{|gg\rangle, |ge\rangle, |eg\rangle, |ee\rangle\}$,

$$\rho_{i,j} = \begin{bmatrix} 1 - |c_{a,i}|^2 - |c_{a,j}|^2 & 0 & 0 & 0 \\ 0 & |c_{a,i}|^2 & c_{a,i}c_{a,j}^* & 0 \\ 0 & c_{a,j}c_{a,i}^* & |c_{a,j}|^2 & 0 \\ 0 & 0 & 0 & 0 \end{bmatrix}. \quad (18)$$

Despite the fact that it is not straightforward to evaluate the entanglement of a mixed state, a simple expression does exist

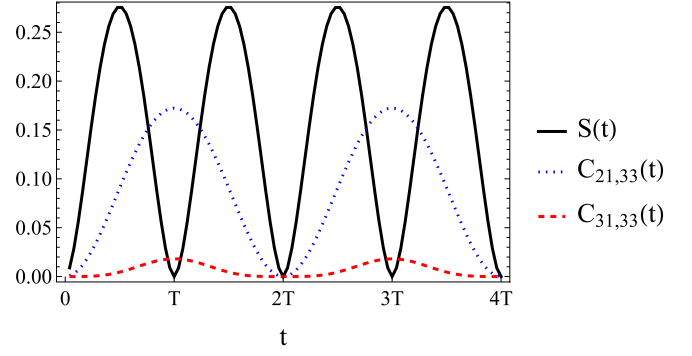


FIG. 2. Exact time evolution of the atom-field von Neumann entropy S and atomic concurrences $C_{x_0,33}$, $C_{31,33}$, for $|\psi(t=0)\rangle = |e_{x_0}\rangle$ with $x_0 = 21$ on a uniform coupled-cavity array featuring $N = 41$ sites operating in the strong-hopping regime with $g = 10^{-3}J$ and $\omega_a = \omega_c$. The entropy oscillates with period $T = \pi/g$.

for an arbitrary state of two qubits. The so-called concurrence is defined by [34]

$$C(\rho_{i,j}) = \max\{0, \sqrt{\lambda_1} - \sqrt{\lambda_2} - \sqrt{\lambda_3} - \sqrt{\lambda_4}\}, \quad (19)$$

where $\{\lambda_i\}$ are decreasing eigenvalues, of the matrix $\rho_{i,j}\tilde{\rho}_{i,j}$, with

$$\tilde{\rho}_{AB} = (\sigma_y \otimes \sigma_y) \rho_{AB}^* (\sigma_y \otimes \sigma_y), \quad (20)$$

and $\rho_{i,j}^*$ being the complex conjugate of $\rho_{i,j}$, and σ_y the Pauli operator. For a separable (fully entangled) state, $C=0$ ($C=1$). Evaluating for Eq. (18), we get

$$C_{i,j} \equiv C(\rho_{i,j}) = 2|c_{a,i}c_{a,j}^*| = 2|\langle e_i|\psi\rangle\langle\psi|e_j\rangle|. \quad (21)$$

B. Time evolution

The protocol starts with a single atomic excitation prepared in the middle of the coupled-cavity system and we let it evolve naturally as $|\psi(t)\rangle = e^{-iHt}|e_{x_0}\rangle$, with $x_0 = \frac{N+1}{2}$ and N being odd so as to have a mode at the center of the band. We set $\omega_a = \omega_c$ ($\Delta = 0$) for now. Note that this triggers a JC-like interaction between the atomic and field modes at that level when in the strong-hopping regime, as discussed in the previous section. Also note that [cf. Eq. (9)] $v_{k, \frac{N+1}{2}} \propto \sin \pi m/2 = 0$ for even m . As the resonance is set at the center of the band, $m = (N+1)/2$ must be an odd number; otherwise there is no propagation when $g \ll J$.

Given the fact that the atomic wave function can only spread out if mediated by the field, the generation of entanglement between pairs of atoms must be preceded by the development of atom-field correlations. We are now to see how this goes for both limiting interaction regimes. The exact entropy dynamics for the strong-hopping regime ($g \ll J$) is depicted in Fig. 2 alongside concurrence for two distinct pairs of atoms. The total atomic probability $\Pi_a(t) = 1 - |v_{k',x_0}|^2 \sin^2(gt)$ and thus the entropy evolves with period $T = \pi/g$, half that of the return probability in Eq. (10). So, two entropy cycles cover (from the beginning) the release of energy from $|e_{x_0}\rangle$ to the photonic degrees of freedom, followed by excitation of the remaining atomic states [see Eq. (11)] at $t = T$ (when $S = 0$), ending up with full recovery of the

initial state at $t = 2T$ via a second transition through the photonic mode. Atomic concurrences set along within the same timescale, reaching its maximum at times $t = T, 3T, 5T, \dots$ in phase, as already implied in Eq. (11). In general, it is crucial to highlight that the degree of entropy generation, as well as the precise timing of the maximum concurrence, are governed by the overlap v_{k',x_0} since communication between atomic and photonic degrees of freedom in the strong-hopping regime involves exchange between $|\alpha_{k'}\rangle$ and $|\beta_{k'}\rangle$ at a single level k' , rather than over the full spectrum. Another feature to note in Fig. 2—also by a careful inspection of Eq. (9)—is that the concurrence involving the atom located at the initial site x_0 overcomes entanglement between any other pair (Fig. 2 shows that for two representative pairs). This is due to the spectral profile of the uniform coupled-cavity array for it restricts the flow out of $|e_{x_0}\rangle$, thereby leaving the remaining cavities with limited resources to establish atomic entanglement, especially for larger N .

Moving on to the the weak-hopping regime ($g \gg J$), we get a whole different picture. Now, there is no special mode triggering the dynamics. All the modes are involved and atomic degrees of freedom are completely mixed with their photonic analogs. Assisted by photonic scattering, the initial atomic excitation spreads out ballistically at rate $J/2$, as $|e_{x_0}\rangle$ is a superposition of even and odd polaritons, both spanning the uncoupled effective chains seen in Fig. 1(d). As it propagates, the atomic wave function is constantly mirrored back and forth to its photonic form in a much faster timescale. In this limit, the entropy is fed with total atomic probability $\Pi_a(t) = \cos^2(gt)$, implying that $S(t)$ reaches its maximum at times $t = m\pi/(4g)$ for odd m [that is, when $\Pi_a(t) = 1/2$]. Note that the above property is general in that it holds for any size N and hopping pattern, with the resulting atomic dynamics always obeying the underlying spectral properties of the coupled-cavity array, as long as g is greater than the free-field bandwidth as well as Δ . Therefore, given that entropy generation is local, generation of atomic entanglement is ultimately driven by wave dispersion. Figure 3 shows some snapshots of the concurrence distribution at times when $\Pi_a(t) = 1$ to get the most of $C_{i,j}$. As one should expect, entanglement is well distributed throughout the array as it evolves, with stronger correlations taking place within each front pulse as well as between them.

Finally, to get a better glance over the spatial distribution of atomic entanglement, in Fig. 4 we display the maximum concurrence recorded within a fixed time interval for all $C_{i,j}$ ($i \neq j$) and covering three different regimes. In the strong-hopping scenario, as a single atomic excitation prepared above the ground state of a uniform coupled-cavity array undergoes a trapping mechanism [23,28,29], it pairs up with each of the remaining atoms to produce the entanglement pattern we see in Fig. 4(a). In this situation, we shall remember that entanglement does *not* spread out from the center of the array (as in Fig. 3); it is generated all at once as the entropy dynamics involves resonant interaction between atomic and photonic delocalized modes (cf. Fig. 2). We observe that such spatial pattern is similar to that of disordered chains reported in Ref. [26], which is very interesting as our array is fully uniform. It means that the atomic trapping mechanism can be thought of as a sort of interaction-induced localization.

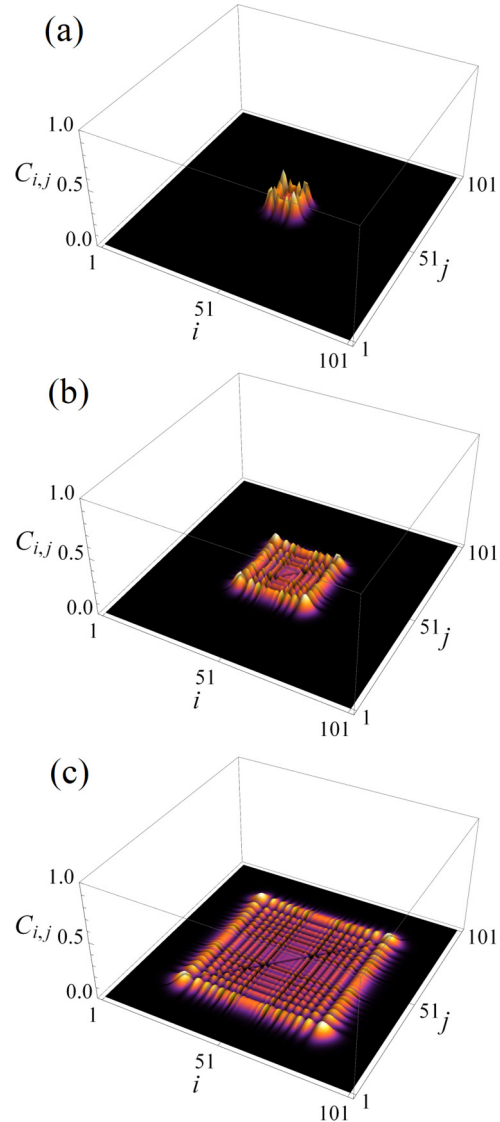


FIG. 3. Snapshots of the atomic concurrence distribution $C_{i,j}(t)$ in the weak-hopping regime for (a) $t = 2000\pi/g$, (b) $t = 5000\pi/g$, and (c) $t = 10000\pi/g$, with $g = 10^3J$, such that $\Pi_a(t) = \cos^2(gt) = 1$ [thus $S(t) = 0$]. The system consists of $N = 101$ coupled cavities with the initial state being $|\psi(t=0)\rangle = |e_{51}\rangle$ and $\omega_a = \omega_c$, and results are exact as obtained directly from Hamiltonian (2). Note that the atomic wave function propagates at rate $J/2$ and thus the front pulse roughly advances a site per J^{-1} elapsed time.

Setting up a moderate interaction strength ($g \sim J$), the entanglement distribution in Fig. 4(b) does not seem to display a very definite pattern, but it marks a crossover to the weak-hopping regime shown in Fig. 4(c). This one is highlighted by the onset of stronger correlations between neighboring atoms as well as between atoms equidistant from the center of the array, as already suggested by Fig. 3. As a full band of extended states begins to take over the dynamics as g is increased, the initial atomic excitation rapidly communicates with the photonic degrees of freedom locally and spreads out, simulating the dynamics of a single photon in an atom-free coupled-cavity array with J replaced by $J/2$ in the limit $g \gg J$. Those maxima in Fig. 4(c) are thus recorded when the front pulse of the atomic wave function passes by [26].

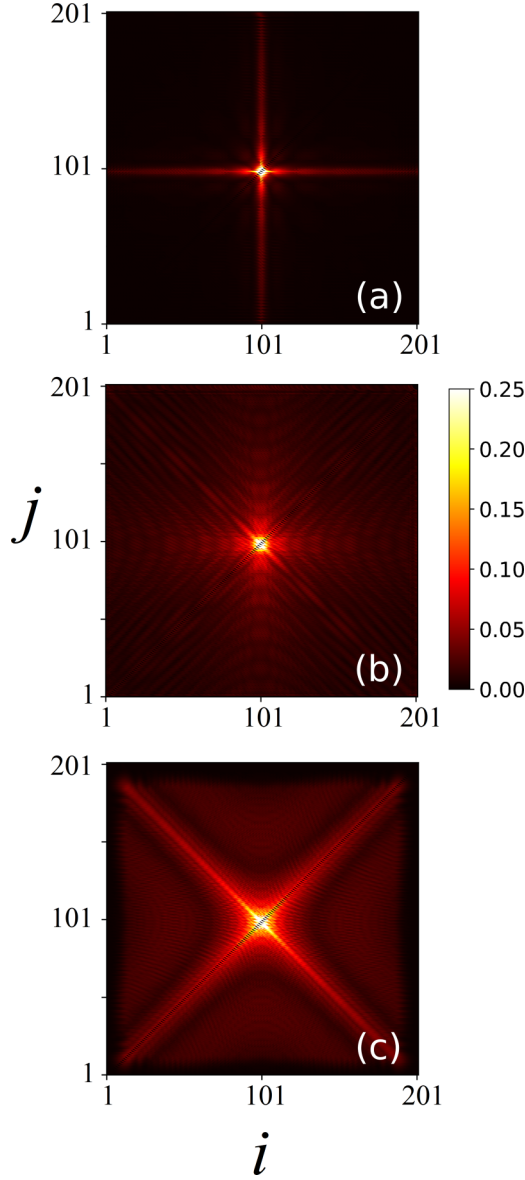


FIG. 4. Maximum concurrence $C_{i,j}(t)$ between all pairs of atoms recorded within time interval $tJ \in [0, 90]$ for three distinct regimes represented by (a) $g = 0.1J$, (b) $g = 1.5J$, and (c) $g = 10J$, considering $N = 201$ cavities and $|\psi(t = 0)\rangle = |e_{101}\rangle$. The time window was chosen so that the wave function did not reach the boundaries in (c). The color map goes from dark to bright as $C_{i,j}(t) \in [0, 0.25]$.

C. Atomic trapping versus Anderson localization

Let us now investigate the behavior of entanglement in the presence of static noise in the cavity frequencies. Consider

$$\omega_c \rightarrow \omega_c(x) = \omega_c + \delta_x \quad (22)$$

in Eq. (1), with δ_x being a random number falling within the boxlike distribution $[-W, W]$, where W is the disorder strength. In particular, we want to address the competition between actual Anderson localization and the atomic trapping that takes place in the strong-hopping regime. Surprisingly, we are about to see that disorder can actually drive the atom-field energy exchange to generate higher levels of atomic-field

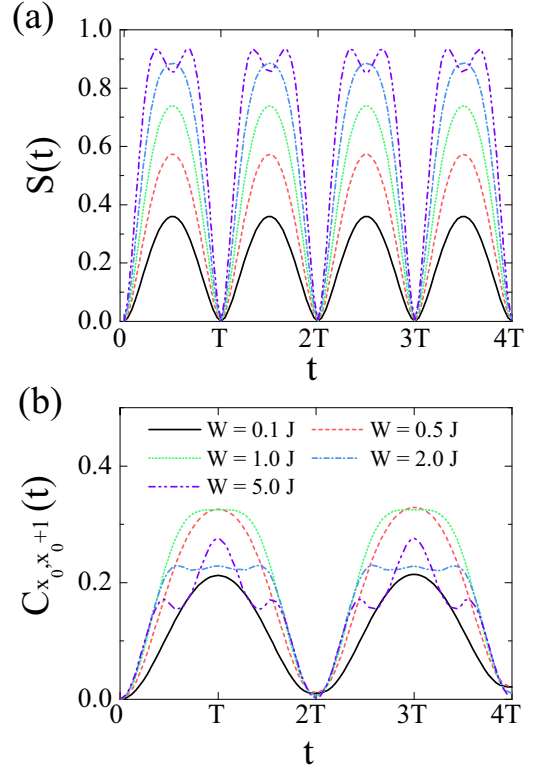


FIG. 5. Exact time evolution of the (a) atom-field von Neumann entropy S and (b) concurrence between the atoms residing at $x_0 = 21$ and $x_0 + 1$ averaged over 10^2 independent realizations of disorder for $N = 41$, $g = 10^{-3}J$, $W/J = 0.1, 0.5, 1, 2, 5$, and with ω_a being set in resonance with the field frequency $\omega_{k'}$ yielding the highest overlap v_{k',x_0} for each sample.

entropy as well as atomic concurrence at short distances when compared to the ordered case.

To see that, first recall that Anderson localization theory establishes that single-particle eigenstates of tight-binding 1D arrays in the presence of on-site uncorrelated disorder are all exponentially localized regardless of the disorder strength [30,35]. This means that the free-field modes are now of the form $v_{k,x} \propto \exp -|x - x_0|/\lambda_k$, where λ_k is the localization length. The outflow of atomic probability from x_0 [see Eq. (10)] should thus be maximized (that is, $p_{a,x_0} = 0$) whenever $|v_{k',x_0}| \geq 1/\sqrt{2}$ at times $gt = \cos^{-1}[(|v_{k',x_0}|^2 - 1)/|v_{k',x_0}|^2]$ in a full period of $2T$. Meanwhile, we also get $\Pi_a(t) = 1/2$ (yielding $S_{\max} = 1$) at times $gt = \sin^{-1}[(\sqrt{2}|v_{k',x_0}|)^{-1}]$, rendering two maxima over an entropy cycle with period T when $|v_{k',x_0}| > 1/\sqrt{2}$. Figure 5(a) shows the time evolution of entropy in the strong-hopping regime (compare to that of the ordered array in Fig. 2) for increasing disorder strengths W averaged over many independent samples. For each one, ω_a was tuned to field frequency $\omega_{k'}$, leading to the highest overlap v_{k',x_0} . Therein, it is remarkable to see that the more intense the disorder is, so is the atom-field entanglement. Also notice that there are indeed two entropy maxima over one full period, meaning that most of the samples are yielding $|v_{k',x_0}| > 1/\sqrt{2}$, as discussed just above, and we are not seeing $S_{\max} = 1$ due to the averaging procedure.

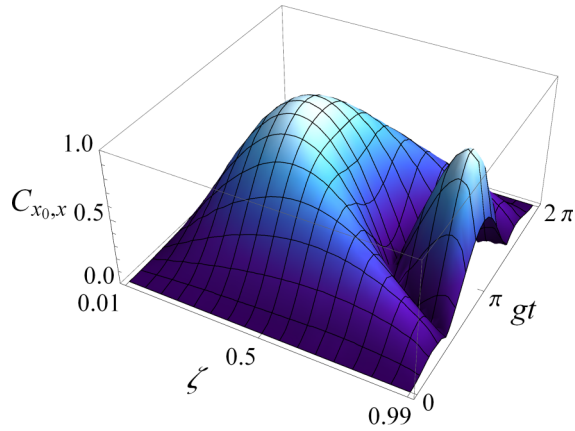


FIG. 6. Analytical concurrence $C_{x_0,x} = 2|c_{a,x_0}, c_{a,x}^*|$ vs time gt and overlap ζ based on the amplitudes in Eqs. (10) and (11) obtained for the strong-hopping ($g \ll J$) regime considering $|v_{k',x_0}| = \zeta$ and $|v_{k',x}| = \sqrt{1 - \zeta^2}$.

We have just confirmed that Anderson localization breaks down the atomic trapping, allowing up to full release of the atomic excitation at x_0 . This provides more resources for generating atom-atom entanglement with its nearest neighbors due to the profile of the involved normal mode. As matter of fact, the concurrence $C_{x_0,x} \propto \exp -|x - x_0|/\lambda_{k'}$ [cf. Eqs. (10) and (11)], and thus we shall focus on the entanglement between the atoms located at x_0 and $x_0 + 1$ to get the most of it. The results are shown in Fig. 5(b) where, once again, disorder acts upon it favorably overall. Note that the concurrence develops some extra oscillations around half period, which is expected due to the interplay between $c_{a,x_0}(t)$ and $c_{a,x}(t)$, and the fact that more amplitude is being released from the atom at x_0 . Another consequence is a nonmonotonic behavior between the maximum concurrence attained in a cycle and W . To better see this, we may feed Eqs. (10), (11), and (21) with $|v_{k',x_0}| = \zeta$ and $|v_{k',x}| = \sqrt{1 - \zeta^2}$, and plot the provisional function

$$C_{x_0,x}(t) = 2|\zeta\sqrt{1 - \zeta^2}[1 + \zeta^2(\cos gt - 1)](\cos gt - 1)| \quad (23)$$

for a range of ζ over a full cycle, as shown in Fig. 6. The above toy model shows that there is a right amount of overlap between the leading mode k' and x_0 able to maximize the concurrence. For this *particular* situation where the available amount of occupation probability to be shared between both atoms is a unit (in general, $|v_{k',x_0}|^2 + |v_{k',x}|^2 \neq 1$ unless there are only two cavities involved), the maximum concurrence is achieved when $|c_{a,x_0}(t)|$ and $|c_{a,x_0}(t)|$ reach $1/\sqrt{2}$ simultaneously. It occurs twice, with the concurrence slowly building up and fading away, with ζ further displaying a sharp revival that would correspond to the strong-disorder regime [compare it to the oscillation patterns in Fig. 5(b) for $W/J = 2.0, 5.0$], thereby explaining the nonmonotonic behavior.

We shall highlight that another interesting feature provided by Anderson localization, still regarding the strong-hopping regime, is that the localization length of the free-field normal modes is maintained for increasing N —and so do the figures of merit for entanglement generation calculated above—whereas for the ordered couple-cavity array, the atomic trapping becomes even worse as v_{k',x_0} diminishes, for the

spectrum is made up by Bloch waves. Analogous behavior was reported by Ciccarello in Ref. [29] using a staggered pattern of hopping rates to induce a discrete, localized mode at the center of the band.

V. CONCLUDING REMARKS

We have studied entanglement generation and its spatial distribution control over a 1D uniform coupled-cavity array described by the JCH Hamiltonian in the single-excitation sector. We carried out detailed analytical calculations for two limiting cases, namely, the weak- and strong-hopping regimes, and set about to study entanglement generation via time evolution of a single atomic excitation prepared above the vacuum (ground) state. We focused on the von Neumann entropy between atomic and field states and the concurrence between pairs of atoms. We found that in the strong-hopping regime ($g \ll J$), entropy generation follows the same timescale as that of concurrence and directly depends on the likelihood of energy release from the emitter located at the initial cavity—which, in turn, depends on the resonant field mode—thus being crucial to make resources available to the other atoms to build up correlations. Due to the Bloch-like spatial profile of the modes involved in the dynamics, an atomic trapping sets in, preventing the initial atom to release its amplitude, thus compromising entanglement generation. By including static disorder in the cavity frequencies, we showed that, curiously, Anderson localization prevents that atomic trapping and allows for maximum atom-field entropy and higher levels of concurrence between the central atom and its neighbors. What is more, it was found that the atomic concurrence responds nonmonotonically to the disorder strength. This sort of interaction-induced localization occurring in the strong-hopping regime is certainly worth further investigation in other scenarios, such as beyond the single-excitation subspace where the photon blockade sets in [19].

In the weak-hopping regime ($g \gg J$), the entanglement dynamics is more straightforward as the entropy oscillates (now between minimum and maximum) much faster than the actual propagation of the atomic wave function, meaning that entropy generation is strictly due to local interactions, differently from the strong-hopping limit. Atomic concurrence then builds up depending on the dispersion profile of the embedded array at rate $J/2$. A uniform one entails ballistic spreading and so the amplitudes are concentrated within the front pulse. Higher degrees of pairwise entanglement are then to be found in between nearest-neighbor atoms, and between them and their equidistant counterpart at the other side of the array in respect to its center.

Although we found that long-distance atomic entanglement becomes weaker due to the dispersive effects of the array itself, it may be distilled into pure singlets [36], to be used in, e.g., quantum teleportation protocols. The natural dynamics of the JCH Hamiltonian may thus be harnessed to generate entanglement between distant nodes in hybrid light-matter quantum network architectures [11,13].

Of course, a more realistic analysis should involve dissipation sources, such as spontaneous emission and photon loss, which could be done via an effective non-Hermitian Hamiltonian upon $\omega_c \rightarrow \omega_c - i\kappa$ and $\omega_a \rightarrow \omega_a - i\gamma$ [37]. That would

simply add an incoherent channel to the vacuum, making the overall occupation probability in the single-particle subspace decay exponentially over time. Therefore, here we are implicitly assuming that each cavity is set in the so-called strong-coupling regime, where $\omega_c, \omega_a \gg g \gg \kappa, \gamma$ so as to fulfill the rotating-wave approximation and allow for many Rabi cycles before the excitation leaves the system. One must thus bear in mind that realization of the strong-hopping regime ($g \ll J$) places some stringent conditions on the dissipation rates. At the other end, for $g \gg J$, this becomes milder, but then the effort turns into keeping the counter-rotating terms neglected. In addition, as in the weak-hopping regime, the atomic concurrence is generated with timescale $\sim J$, and we also need $J \gg \kappa, \gamma$.

Apart from those experimental requirements concerning actual cavity systems, the JCH model may also be explored

through another perspective, namely, that of ladderlike tight-binding chains, as Fig. 1 suggests. There has been a lot of interest in the transport properties of multichannel networks, particularly when the channels are set with different degrees and/or types of disorder, allowing for the engineering of extended states on a disordered background, including the emergence of disorder-free subspaces [38–42]. Here we have seen a remarkable enhancement of entanglement upon placing disorder in the photonic channel, leaving the atomic one unchanged, what leads to further venues of investigation.

ACKNOWLEDGMENT

This work was supported by CNPq, CAPES, FINEP, CNPq-Rede Nanobioestruturas, and FAPEAL.

-
- [1] R. Horodecki, P. Horodecki, M. Horodecki, and K. Horodecki, *Rev. Mod. Phys.* **81**, 865 (2009).
- [2] L. Amico, R. Fazio, A. Osterloh, and V. Vedral, *Rev. Mod. Phys.* **80**, 517 (2008).
- [3] G. Vidal, J. I. Latorre, E. Rico, and A. Kitaev, *Phys. Rev. Lett.* **90**, 227902 (2003).
- [4] A. Osterloh, L. Amico, G. Falci, and R. Fazio, *Nature (London)* **416**, 608 (2002).
- [5] C. H. Bennett, G. Brassard, C. Crépeau, R. Jozsa, A. Peres, and W. K. Wootters, *Phys. Rev. Lett.* **70**, 1895 (1993).
- [6] A. K. Ekert, *Phys. Rev. Lett.* **67**, 661 (1991).
- [7] N. Gisin, G. Ribordy, W. Tittel, and H. Zbinden, *Rev. Mod. Phys.* **74**, 145 (2002).
- [8] C. H. Bennett and S. J. Wiesner, *Phys. Rev. Lett.* **69**, 2881 (1992).
- [9] D. P. DiVincenzo, *Science* **270**, 255 (1995).
- [10] J. I. Cirac, P. Zoller, H. J. Kimble, and H. Mabuchi, *Phys. Rev. Lett.* **78**, 3221 (1997).
- [11] H. J. Kimble, *Nature (London)* **453**, 1023 (2008).
- [12] R. J. Schoelkopf and S. M. Girvin, *Nature (London)* **451**, 664 (2008).
- [13] S. Ritter, C. Nölleke, C. Hahn, A. Reiserer, A. Neuzner, M. Uphoff, M. Mücke, E. Figueroa, J. Bochmann, and G. Rempe, *Nature (London)* **484**, 195 (2012).
- [14] C. Nölleke, A. Neuzner, A. Reiserer, C. Hahn, G. Rempe, and S. Ritter, *Phys. Rev. Lett.* **110**, 140403 (2013).
- [15] A. Reiserer, N. Kalb, G. Rempe, and S. Ritter, *Nature (London)* **508**, 237 (2014).
- [16] A. Reiserer and G. Rempe, *Rev. Mod. Phys.* **87**, 1379 (2015).
- [17] M. J. Hartmann, F. G. S. L. Brandao, and M. B. Plenio, *Nat. Phys.* **2**, 849 (2006).
- [18] A. D. Greentree, C. Tahan, J. H. Cole, and L. C. L. Hollenberg, *Nat. Phys.* **2**, 856 (2006).
- [19] D. G. Angelakis, M. F. Santos, and S. Bose, *Phys. Rev. A* **76**, 031805(R) (2007).
- [20] A. Tomadin and R. Fazio, *J. Opt. Soc. Am. B* **27**, A130 (2010).
- [21] D. Rossini and R. Fazio, *Phys. Rev. Lett.* **99**, 186401 (2007).
- [22] G. M. A. Almeida and A. M. C. Souza, *Phys. Rev. A* **87**, 033804 (2013).
- [23] G. M. A. Almeida, F. Ciccarello, T. J. G. Apollaro, and A. M. C. Souza, *Phys. Rev. A* **93**, 032310 (2016).
- [24] M. Hartmann, F. Brandão, and M. Plenio, *Laser Photon. Rev.* **2**, 527 (2008).
- [25] L. Amico, A. Osterloh, F. Plastina, R. Fazio, and G. M. Palma, *Phys. Rev. A* **69**, 022304 (2004).
- [26] G. M. A. Almeida, F. A. B. F. de Moura, T. J. G. Apollaro, and M. L. Lyra, *Phys. Rev. A* **96**, 032315 (2017).
- [27] T. Fukuhara, S. Hild, J. Zeiher, P. Schauß, I. Bloch, M. Endres, and C. Gross, *Phys. Rev. Lett.* **115**, 035302 (2015).
- [28] M. I. Makin, J. H. Cole, C. D. Hill, A. D. Greentree, and L. C. L. Hollenberg, *Phys. Rev. A* **80**, 043842 (2009).
- [29] F. Ciccarello, *Phys. Rev. A* **83**, 043802 (2011).
- [30] P. W. Anderson, *Phys. Rev.* **109**, 1492 (1958).
- [31] E. T. Jaynes and F. W. Cummings, *Proc. IEEE* **51**, 89 (1963).
- [32] C. D. Ogden, E. K. Irish, and M. S. Kim, *Phys. Rev. A* **78**, 063805 (2008).
- [33] S. Bose, D. G. Angelakis, and D. Burgarth, *J. Mod. Opt.* **54**, 2307 (2007).
- [34] W. K. Wootters, *Phys. Rev. Lett.* **80**, 2245 (1998).
- [35] E. Abrahams, P. W. Anderson, D. C. Licciardello, and T. V. Ramakrishnan, *Phys. Rev. Lett.* **42**, 673 (1979).
- [36] M. Horodecki, P. Horodecki, and R. Horodecki, *Phys. Rev. Lett.* **80**, 5239 (1998).
- [37] H. J. Carmichael, *An Open Systems Approach to Quantum Optics* (Springer, Berlin, 1993).
- [38] S. Sil, S. K. Maiti, and A. Chakrabarti, *Phys. Rev. B* **78**, 113103 (2008).
- [39] F. A. B. F. de Moura, R. A. Caetano, and M. L. Lyra, *Phys. Rev. B* **81**, 125104 (2010).
- [40] A. Rodriguez, A. Chakrabarti, and R. A. Römer, *Phys. Rev. B* **86**, 085119 (2012).
- [41] G. M. A. Almeida, A. M. C. Souza, F. A. B. F. de Moura, and M. L. Lyra, *Phys. Lett. A* **383**, 125847 (2019).
- [42] A. M. C. Souza, G. M. A. Almeida, and E. Mucciolo, *J. Phys.: Condens. Matter* **32**, 285504 (2020).